IEEE Transactions on Geoscience and Remote Sensing
2016, Volume 54 Issue 12 Pages 7339-7350
http://dx.doi.org/10.1109/TGRS.2016.2600239
http://archimer.ifremer.fr/doc/00348/45919/

SMAP L-Band Passive Microwave Observations Of Ocean Surface Wind During Severe Storms

Yueh Simon [1], Fore Alexander [1], Tang Wenqing [1], Akiko Hayashi [1], Stiles Bryan [1], Reul Nicolas [2], Weng Yonghui [3], Zhang Fuqing [3]

[1] Jet Propulsion Laboratory, California Institute of Technology, Pasadena, CA 91109 USA
[2] Laboratoire d'Océanographie Physique et Spatial (LOPS), Institut Français de Recherche et d'Exploitation de la MER (IFREMER), Plouzané, France
[3] the Department of Meteorology and Center for Advanced Data Assimilation and Predictability Techniques, The Pennsylvania State University, University Park, PA, USA

Email addresses : simon.yueh@jpl.nasa.gov ; Alexander.Fore@jpl.nasa.gov ; Wenqing.Tang@jpl.nasa.gov ; Akiko.K.Hayashi@jpl.nasa.gov ; Bryan.W.Stiles@jpl.nasa.gov ; Nicolas.Reul@ifremer.fr ; yhweng@psu.edu ; fzhang@psu.edu

Abstract :

The L-band passive microwave data from the Soil Moisture Active Passive (SMAP) observatory are investigated for remote sensing of ocean surface winds during severe storms. The surface winds of Joaquin derived from the real-time analysis of the Center of Advanced Data Assimilation and Predictability Techniques in the Penn State University support the linear extrapolation of the Aquarius and SMAP Geophysical Model Functions (GMFs) to hurricane force winds. We apply the SMAP and Aquarius GMFs to the retrieval of ocean surface wind vectors from the SMAP radiometer data to take advantage of SMAP's two-look geometry. The SMAP radiometer wind speeds are compared with the winds from other satellites and numerical weather models for validation. The root-mean-square-difference (RMSD) with WindSat or SSMIS is 1.7 m/s below 20 m/s wind speeds. The RMSD with the ECMWF direction is 18 degrees for wind speeds between 12 and 30 m/s. We find that the correlation is sufficiently high between the maximum wind speeds retrieved by SMAP with 60 km resolution and the best track peak winds estimated by the National Hurricane Center and Joint Typhoon Warning Center to allow them to be estimated by SMAP with a correlation coefficient of 0.8 and an underestimation by 8 to 18 percent on average, which is likely due to the effects of spatial averaging. There is also a very good agreement with the airborne Stepped Frequency Radiometer (SFMR) wind speeds with an average RMSD of 4.6 m/s for wind speeds in the range of 20 to 40 m/s.

Keywords : hurricane, microwave remote sensing, ocean surface wind, radar, radiometer

1. Introduction

The near surface ocean wind, generating the momentum flux affecting ocean circulation and mixing, is a key driving force in air-sea interaction processes. Measurement of near surface ocean wind vectors is crucial for many global and coastal oceanographic studies. There are also strong operational and scientific needs in monitoring the surface wind of tropical cyclones. Skillful forecasts of tropical cyclone (TC) track and intensity depend on an accurate depiction of the initial conditions of air and sea states in TC forecast models. A primary source of difficulty in past efforts for TC forecasts has been the inability to make direct observations of the surface wind field, which is one of the key driving forces for the heat and moisture exchanges between air and sea surfaces.

Many spaceborne radiometers and scatterometers with Cto Ka-band frequencies have been operating to make ocean surface wind measurements, but they are limited by reduced sensitivity to wind for hurricane force winds and the impact of rain. It is highly beneficial to develop L-band (~1 GHz) microwave wind radiometers. This is because L-band microwave sensors will be much less susceptible to rain attenuation than higher frequency sensors [1,2] and thus will fill in a critical gap for surface wind observations of severe weather systems. This has been demonstrated by the use of Lband radiometer data from ESA's Soil Moisture Ocean Salinity Mission (SMOS) for hurricane wind speed retrieval [1,2].

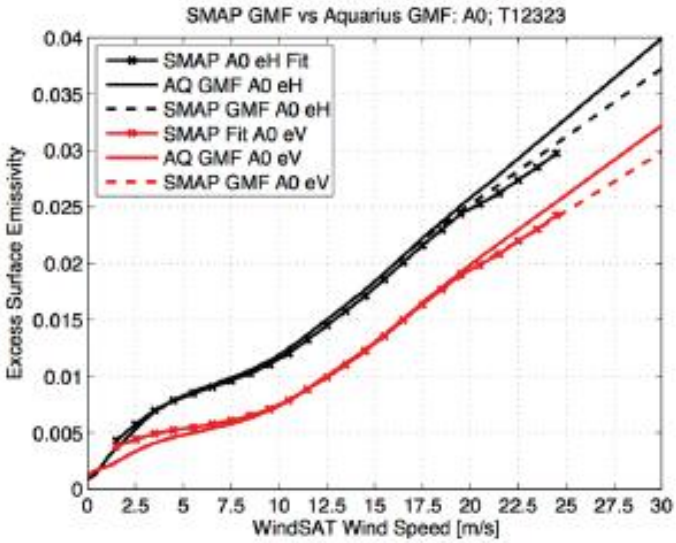

Fig. 1. Excess surface emissivity vs. wind speed for Aquarius and SMAP geophysical model functions.

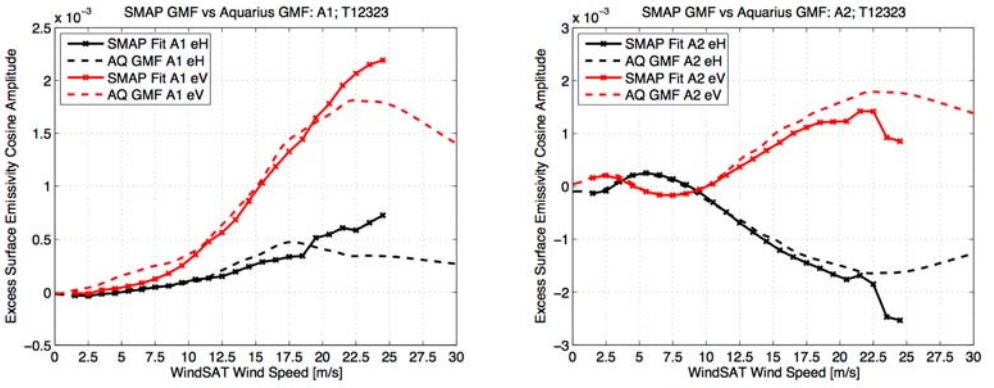

Fig. 2. Amplitude of cosine series fit of excess surface emissivity vs. wind speed for SMAP and Aquarius geophysical model functions. Left panel for A_1 and right panel for A_2.

The NASA Soil Moisture Active Passive (SMAP) observatory was launched January 31, 2015 and started operations in April 2015 to provide global soil moisture and freeze/thaw classification for hydrology and carbon cycle studies [3]. SMAP mission design uses L-band radar and radiometer for collocated, coincident measurements integrated as a single observation system. The radiometer and radar share one common antenna reflector, which is a 6-m mesh deployable antenna. The antenna design consists of an offset parabola reflector with one antenna feed to produce a single antenna beam pointing at an incidence angle of about 40 degrees on the earth surface. The mesh antenna together with the feed is positioned on a spinning assembly to provide observations at two azimuth angles (fore- and aft-looks) with a conical scanning rate of about 14 rotations per minute. The resulting swath width is about 1000 km, which allows global coverage every 3 days.

The SMAP radiometer footprint resolution is ~40 km, while the SMAP L-band radar provides three backscatter products: a full aperture 30x30 km product, a range-sliced product at ~5 km (range) by 30 km (azimuth) resolution, and a Synthetic Aperture Radar (SAR) product at higher resolution (~1 to 3 km). The SMAP instruments have been calibrated using the data from other satellites and external targets. The calibration of the SMAP radiometer noise diode was achieved using the ocean targets and cold sky. Cross-comparison with SMOS radiometer data [4] over land and ocean surfaces indicates an excellent agreement of about 1 K.

II. Characteristics of SMAP radiometer singals for high winds

We perform matchups of the SMAP radiometer data (L1B surface TB) with ancillary data, including the ocean wind direction from the National Center for Environment Predictions (NCEP) [5], wind speed from WindSat and the Special Sensor Microwave Imager/Sounder (SSMIS) [6], HYCOM's sea surface salinity (SSS) [7], and Reynolds sea surface temperature (Ts) [8]. The method of matchup and ancillary data is the same as what have been described in [9,10]. The matchup is performed globally for the data collected from April 2015 through February 2016. We subtract the flat surface emission (T_{Bpflat}) from the data, bin the difference as a function of wind speed and direction at 1 m/s in wind speed and 10^o in direction intervals, and then perform the harmonic analysis to model the vertically and horizontally polarized excess brightness temperatures, T_{BV} and T_{BH}, respectively, by the following three term cosine series.

$$e_p = \frac{T_{Bp} - T_{Bpflat}}{T_s} = A_{0p}(w) + A_{1p}(w)\cos\phi + A_{2p}(w)\cos 2\phi \quad (1)$$

where w is the surface wind speed and ϕ is the relative direction between the SMAP look direction and wind direction. The subscript, "p", indicates the polarization, vertical (V) or horizontal (H).

We find that the harmonic coefficients (A_i) derived from the SMAP data are in good agreement with the Aquarius geophysical model function (GMF) derived from the matchup data up to a wind speed of 20 ms^{-1} (Figs. 1 and 2). The SMAP excess surface emissivities, A_{0p}, are illustrated in Fig. 1 together with the corresponding Aquarius data and GMF [9,10]. For wind speeds above 20 m/s, it appears that SMAP data have a slightly smaller sensitivity than Aquarius. The small difference at high wind speeds could be due to the differing time periods and durations of SMAP and Aquarius data records: Aquarius operated from September 2011 through early June 2015 for a duration of 3 years and 9 months, while SMAP data acquisition started in April 2015. The duration of SMAP data, about a year, may not provide sufficient matchups above 20 m/s for accurate estimation of A_0. It should be noted that the shape of GMF curve depends on the wind speed product used for conditional matchup. Should the NCEP wind speed be used, the slope of the curves will be greater because the NCEP wind tends to provide lower wind speed than the WindSat or SSMIS for high winds.

The wind direction dependence of excess surface emissivity is modeled by A_1 and A_2 coefficients, which are illustrated versus wind speed in Fig. 2. The values estimated from SMAP data are noisy above 20 m/s wind speeds. This provides further evidence that there are insufficient SMAP data samples above 20 m/s for accurate modeling analysis. In any case the agreement between the SMAP data and the

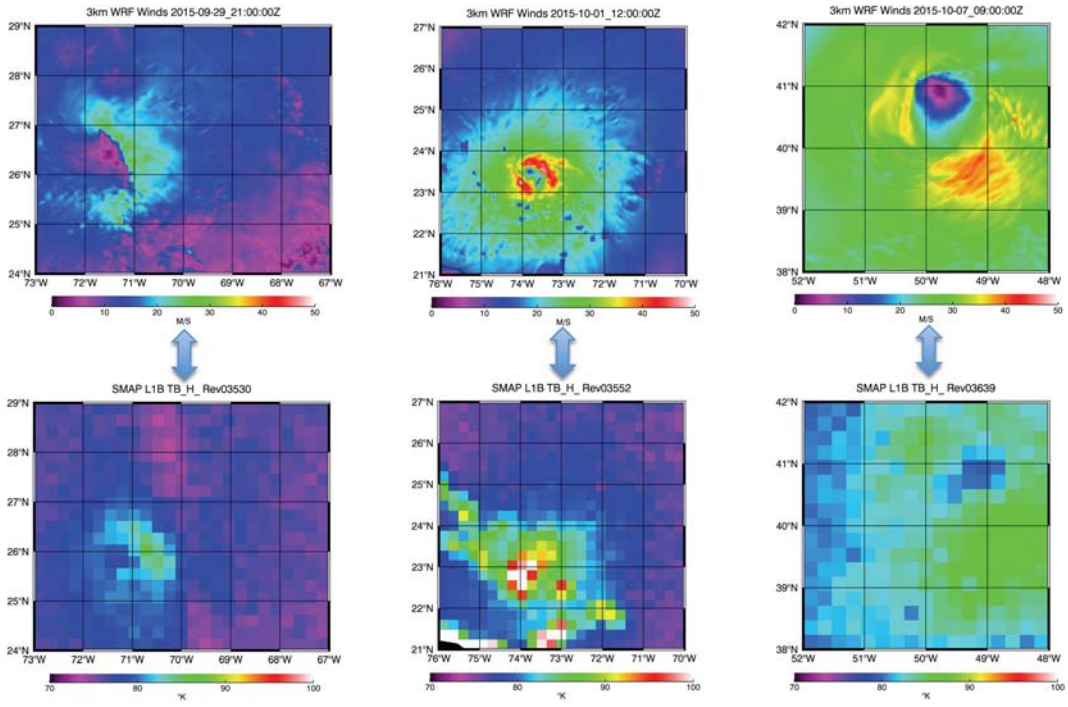

Fig. 3. SMAP brightness temperatures (lower panels) and APSU winds (upper panels) for hurricane Joaquin on Sept. 29, Oct. 1, and Oct. 7, 2015.

Aquarius GMF is reasonable below 20 m/s wind speeds. Due to insufficient SMAP data for high winds (above 20 m/s) and reasonable agreement with Aquarius at lower wind speeds, we constructed the first version of SMAP GMF by adjusting the slope of Aquarius model A_0 to fit the SMAP data indicated in Fig. 1 and inheriting the Aquarius model coefficients for A_1 and A_2.

The directional variation in SMAP T_B for high winds can be about 1 to 1.5 K in the wind speed range of 15 to 25 m/s, as indicated in the Aquarius data [9,10]. It is seen in Fig. 2 that the values of A_2, characterizing the upwind and crosswind differences, can be close to 0.002, which corresponds to about 0.6 K for warm waters with a temperature of about 25°C. The value of A_1 for vertical polarization can also reach about 0.002 at wind speeds above 20 m/s. The directional variation in L-band T_{BV} and T_{BH} data is not significant in comparison with the Noise Equivalent Delta T (NEDT) of 1.1 K for the SMAP radiometer data averaged over 11.2 ms [3]. The data have to be further averaged to reduce the NEDT for wind speed and direction retrieval.

To explore the dependence of excess T_Bs on wind speed for severe wind conditions, we utilize the surface wind analyses of Hurricane Joaquin (2015). The surface wind is derived from the real-time analyses provided by the Center of

Table 1. SMAP Data And APSU WRF Wind Matchup.

SMAP Rev/Time (Date/hh/mm)	APSU WRF
3530A/0929T2149	2015-09-29_21Z
3545A/0930T2226	2015-09-30_21Z
3552D/1001T1045	2015-10-01_12Z
3574A/1002T2202	2015-10-02_21Z
3603A/1004T2137	2015-10-04_21Z
3639D/1007T0931	2015-10-07_09Z

Advanced Data Assimilation and Predictability Techniques (ADAPT) at the Penn State University (PSU). The ADAPT/PSU hurricane analysis and prediction system (APSU) uses an ensemble Kalman-filter (EnKF) for data assimilation based on the Weather Research and Forecasting (WRF) model. The system configuration and data assimilation methodology are the same as those in [11,12] except for updating the WRF model to version 3.5.1. The WRF model has 43 vertical levels and 3 two-way-nested domains with horizontal grid spacings of 27, 9, and 3 km, covering areas 10,200 km × 6,600 km, 2,700 km × 2,700 km, and 900 km × 900 km, respectively. For Hurricane Joaquin (2015), the system is initialized at 0000 UTC 28 September 2015 with 60 ensemble members perturbed with Global Forecast System

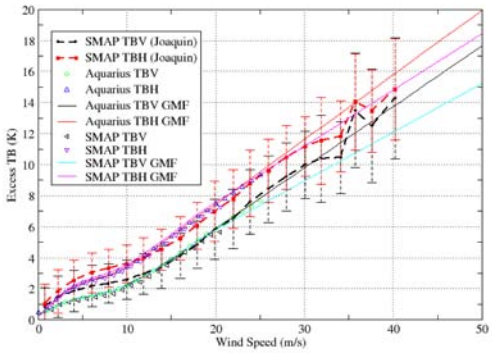

Figure 4. Comparison of SMAP and Aquarius geophysical model functions and data with the matchup of SMAP-APSU winds of Hurricane Joaquin. The excess TBs from Aquarius and SMAP GMFs are evaluated at 300 K for the surface temperature.

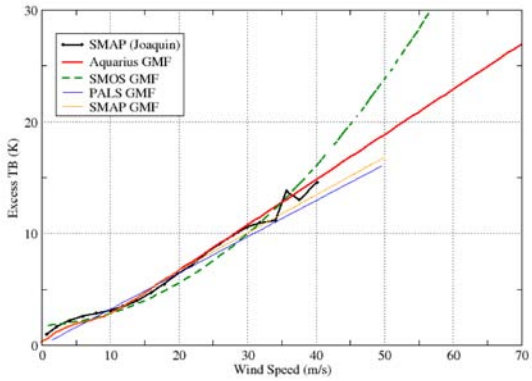

Figure 5. Comparison of SMOS, SMAP, Aquarius, and Airborne PALS geophysical model functions for the average of T_{BV} and T_{BH}. The excess TBs from all GMFs are evaluated at a surface temperature of 300 K.

(GFS) analysis, after 12 h free ensemble forecast, the system starts cycling data assimilation at 1200 UTC 28 September till the end of the hurricane life at 1500 UTC 7 October 2015 with a 3-h assimilation window. The real-time assimilated observations include all conventional observations, satellite derived winds, dropsondes collected by Meteorological Assimilation Data Ingest System (MADIS, https://madis.noaa.gov/), High-Density Observations (HDOB) of aircraft reconnaissance, and the minimal sea-level pressure from the Tropical Cyclone Vital Database (TCVitals), which contains tropical cyclone location, intensity, horizontal wind and pressure structure, and depth of convection and is generated in real-time every 6 h by forecasters. More details about the APSU system can be found in [12].

Fig. 3 provides a visual comparison of the SMAP T_B data with the APSU analyses. The bottom panels illustrate the SMAP T_{BH} data from revs 3530A, 3552D, and 3639D gridded on a 0.25 degree grid in latitude and longitude. The letters "A" and "D" after the rev number stand for ascending and descending orbits, respectively. The upper panels of Fig. 3 illustrate the corresponding 3-km resolution APSU surface winds of Joaquin on Sept. 29 at 21 UT, Oct 1 at 12 UT, and Oct 7 at 9 UT. The time difference from SMAP observations is within one and a half hour (Table 1). The maximum APSU wind speed is about 30 m/s on Sept 29; the corresponding SMAP T_{BH} data from rev 3530A have a good agreement with the APSU winds, indicating generally higher T_Bs for higher wind speeds, and the T_Bs in the eye region are slightly lower than that in the surrounding areas. The APSU winds (upper middle panel in Fig. 3) for the SMAP pass (rev 3552D) on Oct 1, 2015 have exceeded 40 m/s. In this case, the eye of hurricane has become clearly identifiable in the wind image. Although the eye cannot be resolved in the SMAP T_B image (lower middle panel in Fig. 3) due to a lack of spatial resolution, the SMAP T_Bs tend to have an increasing trend from far away to near the eye, indicating the dependence of T_B on wind speed. There are some regions of moderate wind speeds (blue) with high SMAP T_Bs (color coded in red or white); these regions correspond to the locations of some of the islands in the Caribbean, where land T_Bs are high. On 7 October 2015, Joaquin became an extra-tropical storm. Its eye became quite large, reaching about 100 km in diameter (Upper right panel in Fig. 3). The region of maximum wind (about 40 m/s) is located to the southeast of the eye. The SMAP T_B data (lower right panel) reveal similar spatial patterns, and the hurricane eye can now be resolved by the SMAP radiometer.

We interpolated the best track analysis in time to estimate the position of cyclone at the time of SMAP passes. The APSU analyses before and after the SMAP passes were shifted to the estimated position, and then the APSU winds were interpolated in time to the SMAP footprint location. The 3 km APSU winds were averaged to match the SMAP footprint size of 40 km. Our analysis includes six revs of SMAP data (Table 1); with the exception of rev 3545A, all revs have the eye of Joaquin located in the swath. The matchup data are conditionally binned on the APSU wind speed at 2 m/s intervals. The mean and standard deviation of the SMAP T_B data in each bin are computed and illustrated in Fig. 4. Note that we have included only matchup bins with at least 5 data points in Fig. 4. The linear extrapolations of SMAP and Aquarius GMFs to the wind speed range of 25 to 40 m/s are within the error bars of the SMAP-APSU analysis.

We have compared the Aquarius and SMAP GMFs with the SMOS GMF for hurricane force winds [2] (Fig. 5). The excess T_Bs from the GMFs are evaluated at a surface temperature of 27°C (or 300 K). The SMOS GMF for hurricane wind retrieval characterizes the average of T_{BV} and T_{BH} with a parabolic dependence on wind speed. These three models agree reasonably well with each other for wind speeds lower than 35 m/s although the SMOS GMF produces a smaller excess T_B by about 1 K at 20 m/s. At wind speeds of 35 m/s or higher, the SMOS GMF takes a sharp rise, deviating from the SMAP and Aquarius GMFs, which are a linear extrapolation of data from lower wind speeds. In Fig. 5 we

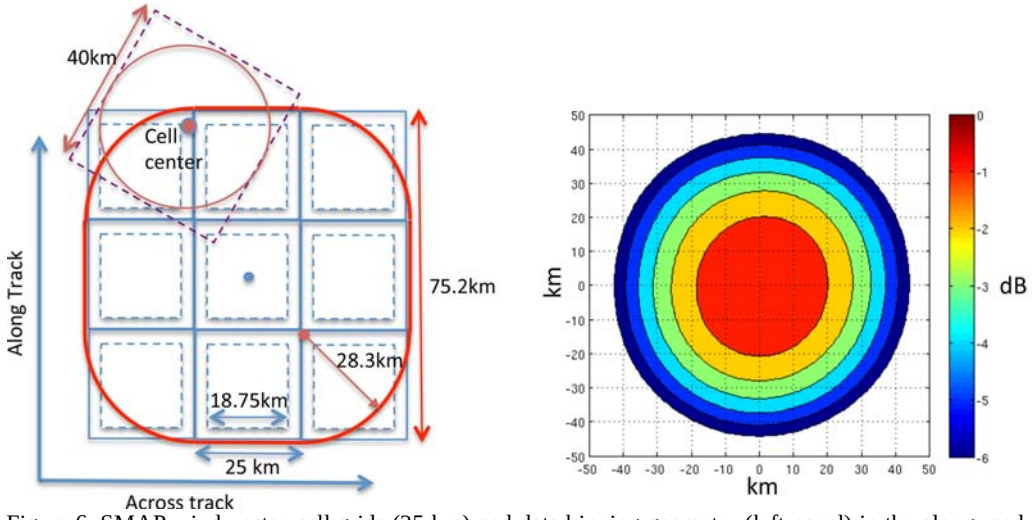

Figure 6. SMAP wind vector cell grids (25 km) and data binning geometry (left panel) in the along- and across-track coordinate system. The averaged power pattern of binned radiometer data under the assumption that the center of the data point can be randomly distributed in the red contour.

have included the GMF derived from the airborne Passive-Active L-band System (PALS) data acquired during a campaign in the North Atlantic in 2009 [13]. The PALS GMF, which is a linear regression model of data acquired below 30 m/s near a surface temperature of 3°-5°C, has been adjusted to predict the excess T_B at the surface temperature of 300 K. The PALS model agrees well with the SMAP GMF. However the SMAP-APSU analysis seems to be closer to the Aquarius GMF. At this point, the uncertainty of the SMAP-APSU analysis of data from Joaquin with the error bars indicated in Fig. 4 does not allow us to discriminate the relative accuracy of SMOS, SMAP and Aquarius GMFs. The error bars in Fig. 4 correspond to about 3 K of excess brightness temperature at the wind speed of 40 m/s. The curves for the SMOS, Aquarius and SMAP GMFs in Fig. 5 are within the error bars of 3 K, which are not noted on Fig. 5.

Our analysis indicates significant discrepancies among the geophysical model functions above wind speeds of 40 m/s. The discrepancy could be caused by differences in the reference wind data and angle of observations for analysis. The SMOS GMF analysis performed by [2] uses the H*Wind analysis [14], while the APSU wind is used in our analysis of SMAP data. Furthermore, the SMOS GMF is an average of excess brightness temperatures over the incidence angles from 10 to 60 degrees, while the SMAP data are at the incidence angle of 40 degrees. We don't expect the incidence angle effects to be significant, but would like to note it here for completeness. Future analyses should include extensive matchups with category 4 and 5 storms using the same surface wind analysis and limit the range of SMOS data to near the incidence angle of 40 degrees to enable a consistent comparison.

III. Ocean Surface Wind Retrieval

We apply the SMAP and Aquarius GMFs to the retrieval of ocean surface wind from the SMAP radiometer data by leveraging the QuikSCAT algorithms to account for the two-look geometry (fore and aft looks from the conical scan) and dual-polarization observations. The SMAP radiometer data are binned on rectangular grids at 25 km spacing with their axes aligned with the along and across track directions of satellite (Fig. 6). To account for the directional dependence we average the data separately for the data collected from fore and aft looks, therefore reducing the data into two looks.

We follow the gridding approach used for QuikSCAT data processing [15] with the geometry illustrated in Fig. 6. In each wind vector cell (WVC) of 25 km resolution, indicated by a blue box, there is a smaller box with its borders (dashed lines) shorter than that of the WVC by 25 percent. For each SMAP footprint cell, we define a 40 km by 40 km square box (orange borders) with its orientation corresponding to the azimuth direction of SMAP observation. If any edge of the square box has intercepts with the dashed lines in the WVC, then the data will be included for wind processing. This gridding scheme allows the binning of any SMAP data with its footprint center in the red contour with a width of about 75 km. Because of the conical scanning geometry of SMAP, the orientation and relative location of the gridded SMAP footprints with respect to the center of WVC can have a large variation across the swath. We perform a statistical estimation of the effective wind product resolution by computing the averaged power of gridded data under the condition that the footprints can be randomly located and oriented in the red contour. We represent the power pattern of each footprint by a Gaussian beam with a half power width of 40 km. The integrated power pattern of all possible footprint positions and orientation is indicated in the right panel of Fig. 6 with 1 dB color-coded contour intervals. It is known that the fraction of power within the 3 dB beamwidth of a two-dimensional Gaussian beam is 50 percent. Therefore we find the mean radius of the contour, which encloses 50 percent of the integrated power, and define it as the effective resolution of

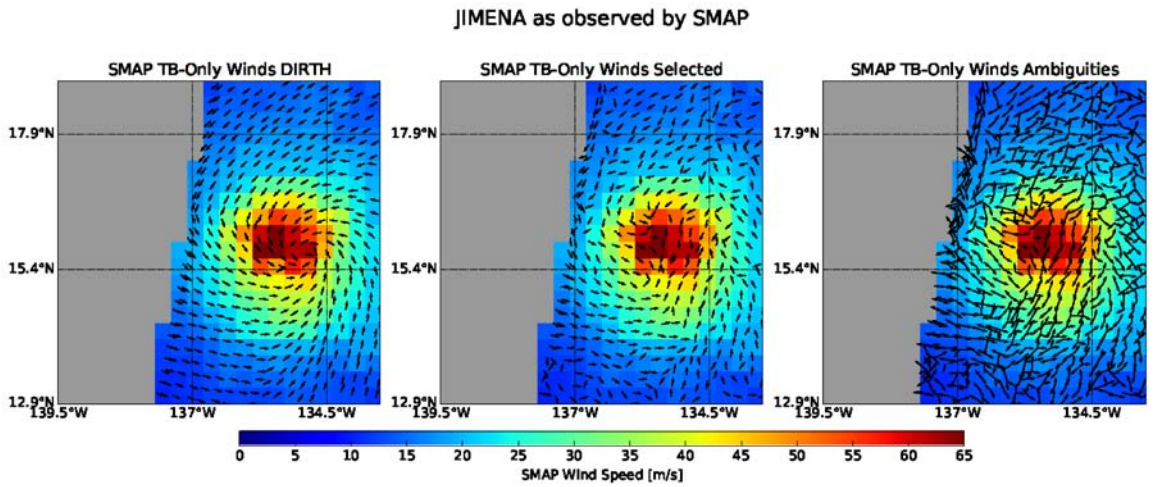

Figure 7. SMAP wind ambiguities (right panel), selected ambiguity (middle) and DIRTH solution (left panel) for Hurricane Jimena on August 31, 2015. The best track wind speed of Jimena is 66 m/s.

gridded data. The mean radius of this 50 percent contour turns out to be 30 km from the center of WVC. This leads to the conclusion that the effective resolution of gridded data is 60 km.

We use the following quadratic cost function for retrieving the hurricane wind speed (w) and direction (ϕ) from T_{BV} and T_{BH}:

$$C_{HW}(w,\phi) = \sum_{i=1}^{2} \frac{(T_{BVi} - T_{BVMi})^2}{\Delta T_{BV}^2} + \sum_{i=1}^{2} \frac{(T_{BHi} - T_{BHMi})^2}{\Delta T_{BH}^2} \quad (2)$$

The T_{BVM} and T_{BHM} represent the values computed form the SMAP or Aquarius GMF. The subscript "i" represents the data from two looks (fore and aft). The weighting coefficients, ΔT_{BV} and ΔT_{BH}, correspond to the noise-equivalent-delta-temperature (NEDT) of radiometer observations.

In the cost function, the SMAP data, T_{BV} and T_{BH}, are the surface brightness temperatures after the antenna pattern correction (inc. reflection of galactic radiation and sun glint), correction of atmospheric attenuation and emission, and Faraday rotation correction [16]. The Faraday rotation correction was accomplished using the third Stokes data (U) acquired by SMAP under the approximation that the 3rd Stokes emission from ocean surfaces is negligible [17].

Through the analysis of Aquarius data, it is known that the wind direction signal in the third Stokes emission from sea surfaces at L-band frequencies is 1 K or less [9]. Since the 3rd Stokes data will be significantly affected by the Faraday rotation [17], accurate ancillary ionospheric total electron content (TEC) data and earth magnetic model field have to be introduced to correct the Faraday rotation effects on U before it can be used for vector wind retrieval. Although the TEC data products have been produced from the Global Positioning Satellite (GPS) data, they contain the TEC from the altitude of GPS satellites to the surface, more than the TEC under the SMAP orbit altitude. Because additional modeling is required to estimate the TEC under the SMAP satellite orbit in order to remove the Faraday rotation effects from the third Stokes, we don't include the third Stokes data in the cost function for vector wind retrieval.

An alternate approach to consider the third Stokes data is to introduce the quantity $Q_p = \sqrt{(T_{BV} - T_{BH})^2 + U^2}$ in the cost function for retrieval. It is known that Q_p is insensitive to Faraday rotation [17]. However Q_p is nearly insensitive to the wind direction modulation in U. At the incidence angle of 40 degrees, T_{BV}-T_{BH} of ocean is about 40 K, whereas the amplitude of U caused by wind direction is about 1 K or less [9]. Using a Taylor series expansion, we find that

$$Q_p \sim T_{BV} - T_{BH} + \frac{U^2}{2(T_{BV} - T_{BH})} \quad (3)$$

The second term for sea surfaces will be nominally smaller than 1/80=0.0125, which essentially has no contribution to Q_p. Introducing Q_p in the cost function will bring in essentially no new information from the third Stokes data (U) for wind retrieval.

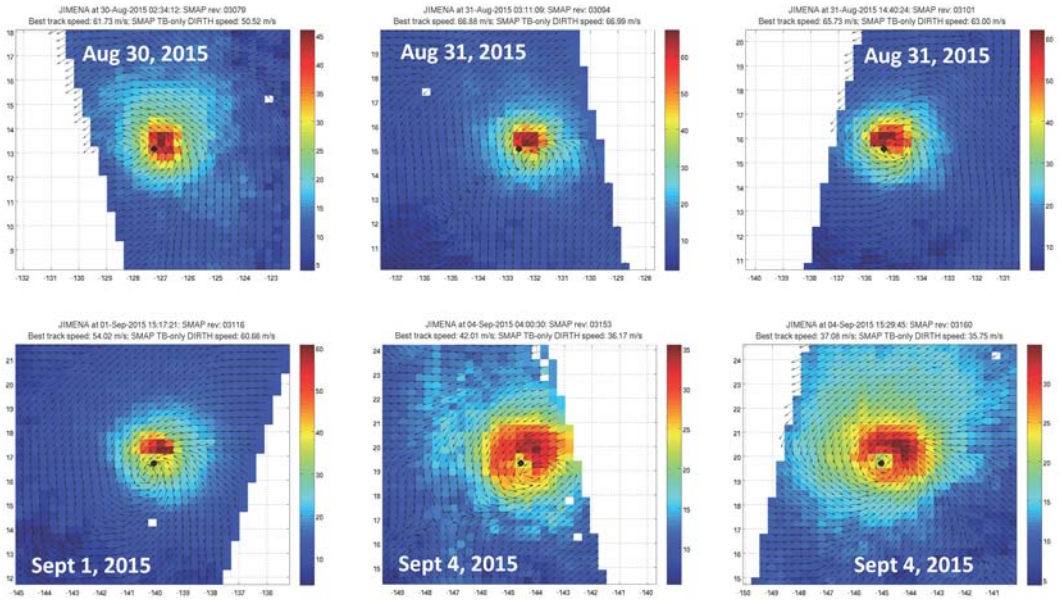

Figure 8. SMAP radiometer wind vector images of Hurricane Jimena from August 30 to September 4, 2015.

In addition to the third Stokes, SMAP radiometer also makes measurements of the fourth Stokes parameter data [2,16], which characterizes the imaginary part of the complex correlation between vertical and horizontal polarizations. Based on high frequency (18 GHz) radiometer data acquired in the past, the fourth Stokes is typically a factor of two or more smaller than the third Stokes [18]. The expected small amplitude of the fourth Stokes data at L-band for sea surfaces will require significant effort to separate the instrumentation errors and may require further spatial averaging to reduce NEDT for wind retrieval. When more SMAP data become available, particularly for high winds, it will then be possible to develop a geophysical model function of the fourth Stokes data and then assess its impact on wind retrieval.

For the wind speed and direction retrieval algorithm using the cost function defined by Eq. (2), we provide the ancillary SSS from HYCOM as input to the geophysical model function because T_Bs of vertical and horizontal polarizations essentially have the same sensitivity to wind speed above 20 m/s and consequently do not allow simultaneous wind speed, wind direction, and salinity retrieval. In general, there are multiple local minima (ambiguities) in the 2-dimensional speed and direction space. To improve the consistency of directional retrieval in the swath, we apply a combination of median filtering technique for ambiguity removal [19] and the Directional Interval Retrieval with THreshold (DIRTH) nudging technique developed for QuikSCAT wind processing [20]. See Fig. 7 for an example of the SMAP wind ambiguities, median filtering and DIRTH processing for Hurricane Jimena.

The ambiguity removal process begins with a DIRTH type of processing [15], where we retrieve a best wind speed value for every direction and identify the ambiguities as the local minima of the objective function. Then we convert the objective function values (C_{HW}) to pseudo-probability density function (PDF$\sim e^{-C_{HW}(w,\phi)}$) and build out direction intervals about each ambiguity so that a threshold value of the total pseudo-PDF is contained in the union of the direction intervals. We then search for the threshold PDF value such that 99% of the integrated probability is comprised of PDF values larger than this threshold value. The portions of the curve above this PDF threshold value are used to build the direction intervals about each ambiguity [20].

The local minima in the objective function values are not very deep for winds below 15 m/s as the direction signal in the T_B GMF is not large for low to normal winds. Typically we would obtain 2 ambiguities for normal wind speeds. However, for high wind we obtain up to 4 ambiguities

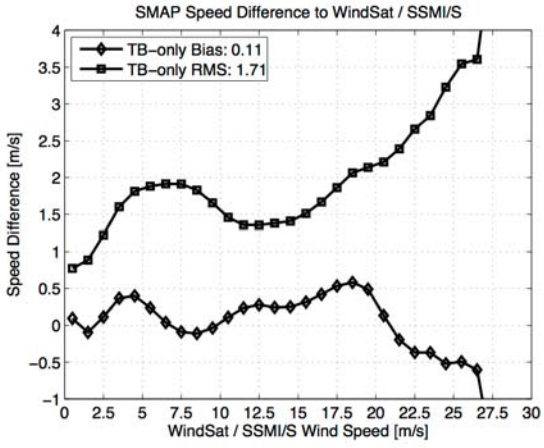

Fig. 9. Comparison of the SMAP radiometer wind speed with the WindSat and SSMIS wind speeds; diamonds for bias and squares for RMSD.

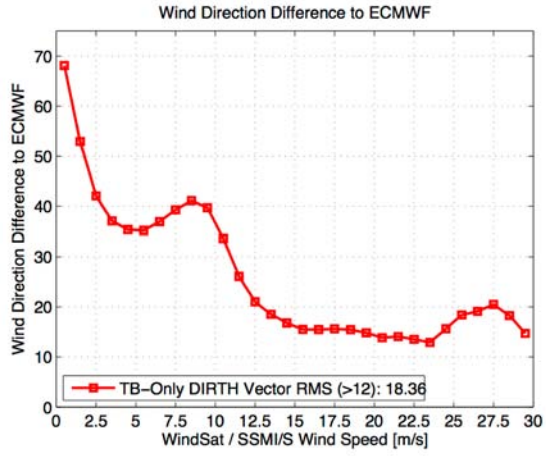

Figure 10. Comparison of the SMAP radiometer wind direction with the ECMWF wind direction.

as the direction modulation of the T_B is more significant for high winds. See the right panel of Fig. 7 for examples of directional ambiguities.

Next we perform the ambiguity removal process to select among the multiple minima obtained in the previous step. To perform the ambiguity removal, we first initialize the selected ambiguity wind field with the ambiguity that is nearest to the NCEP Global Data Assimilation System (GDAS) wind vector. Next we perform an iterative spatial median filtering ambiguity removal process [19] where each WVC's ambiguity for the next iteration is set to the nearest ambiguity to the surrounding 2-dimensional (7x7 window) median of the current iteration's selected ambiguity wind field. This process is repeated until the number of changes in WVC converges or a maximum iteration counter (200) is reached.

Then we perform the final portion of the DIRTH processing [20] where the ambiguity is fixed but the direction is allowed to vary within the direction intervals identified in the first step of the processing. We iteratively relax the wind direction solutions to be the direction nearest to the surrounding vector median and repeat until the direction selections converge or a maximum iteration counter of 200 is reached.

Figure 8 illustrates the SMAP wind images of Hurricane Jimena in late August-early September 2015. Jimena was a category-4 hurricane with its maximum wind speed reaching 140 knots (or about 70 m/s) in late August. The SMAP wind direction appears reasonable, indicating closed circulation of winds around the eye. The center of closed circulation agrees with the position of best track (black dots), except for the data acquired on August 30 and 31. The National Hurricane Center (NHC) best track data show that Jimena grew significantly in intensity from August 27 to 30, and the hurricane was near its peak strength on August 31 and September 1. The temporal change in intensity is reflected in the images. (Note that we have adjusted the color scale for each panel in Fig. 8 to maximize the wind speed contrast.) While Jimena was strengthening, its vortex seemed to have tightened up between August 30 and 31, and the eye was not resolvable by the SMAP radiometer. The subsequent images reveal that the vortex grew larger over time with its diameter reaching about 50 km on Sept 4. The evolution of hurricane size agreed with the best track analysis, which indicated that the radius of maximum wind evolved from 37 km at the end of August 30 to about 28 km on 31st, and became 46 km on Sept. 4. The wind images for Jimena also reveal that the wind patterns are asymmetric around the eye with the regions of maximum wind generally located to the right hand side of the track; this asymmetric feature is primarily due to the forward motion of hurricane added to the inflow of surface winds toward the eye. Overall the features of SMAP radiometer wind vectors of Jimena appear reasonable. However there is no accurate in-situ data for validation.

IV. Validation

We assess the SMAP radiometer winds in two wind speed regimes, 1) one for wind speeds lower than 20 m/s and 2) the other for higher wind speeds, by comparison with the wind products from other satellites, airborne and numerical weather models. For the lower wind speed regime, we carry out a comparative analysis with the wind speeds from WindSat or SSMIS and the wind direction from the European Center for Medium Range Weather Forecasts (ECMWF). For the high wind regime, we apply the best track analysis for comparison of wind structure maxima, and make comparison with the operational airborne Stepped Frequency Microwave Radiometer (SFMR) winds for hurricanes [21].

We collocate the SMAP radiometer wind with the ECMWF wind by temporally interpolating the ECMWF winds before and after the SMAP pass. For the WindSat and SSMIS collocation, the data acquired within 15 minutes is used. The bias and standard deviation of the SMAP radiometer wind speed product computed with respect to the WindSat or SSMIS wind speed are compared in Fig. 9. The bias (diamonds in Fig. 9) is under 0.5 m/s over the wind speed

the

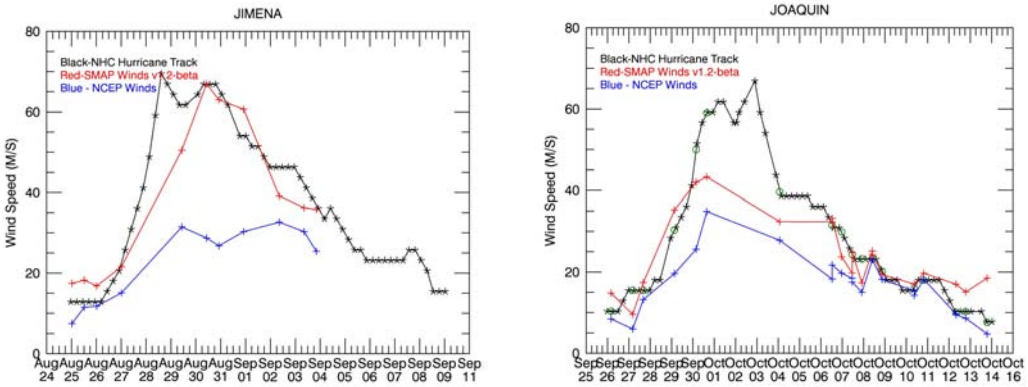

Figure 11. Time series of the maximum wind speeds of Hurricane Jimena (left) and Joaquin (right) estimated from the SMAP radiometer data (red crosses), best track analyses (black stars), and NCEP (blue crosses). SMAP has captured the peak of Jimena, but missed the peak of Joaquin on Oct 1-2.

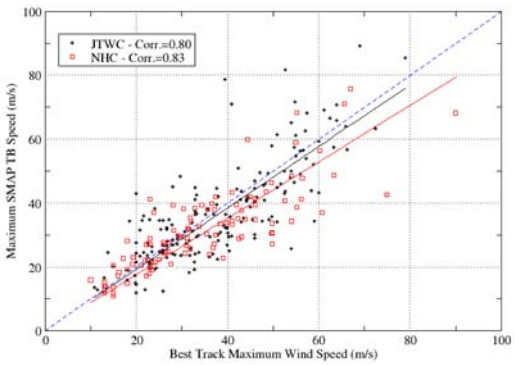

Figure 12. Comparison of maximum wind speed indicated in the SMAP data with the best track analysis from the Joint Typhoon Warning Center (JTWC) (black dots) and National Hurricane Center (NHC) (red squares). The blue diagonal line represents the one to one reference. The black and red solid lines correspond to the linear regression of the scattered SMAP-Best Track data for JTWC and NHC, respectively.

range of 0 to 20 m/s, and the RMSD (squares) is about 1.7 m/s. The RMSD could be caused by the residual NEDT of gridded data and error in the ancillary data. The HYCOM SSS is known to have a saltier bias in parts of Eastern Pacific and Western Atlantic where precipitation and freshwater plume from river discharge are significant for the surface salinity. The large RMSD of about 2 m/s in the range of 5 to 8 m/s could be the result of reduced sensitivity of excessive surface emissivity to wind speed. It is evident in Fig. 1 that the slopes of the excess surface emissivity curves are smaller in this wind speed range than lower or higher wind speeds.

The RMSD between the directions of SMAP radiometer wind and ECMWF analysis is illustrated in Fig. 10. The RMSD is larger than 20 degrees for wind speeds below 12 m/s, but reaches to as low as 15 degrees at about 20 m/s wind speeds. The overall RMSD is 18.4 degrees for wind speeds in range of 12 to 30 m/s. The comparison indicates that the SMAP radiometer can provide reasonably accurate ocean direction for high winds corresponding to tropical depression and tropical storm intensities (12 to 30 m/s).

The assessment of SMAP radiometer wind speed above hurricane force (>33m/s) is performed by comparison with the maximum wind speed in the best track (BT) analysis for all storms that have reached above category 1 during their lifetime. There are 22 storms with the NHC BT analyses, and 32 storms with the Joint Typhoon Warning Center (JTWC) BT analyses through the end of March 2016. We have obtained a total of 105 SMAP passes for comparison with the NHC BT, and 172 passes with the JTWC BT. These storms include many category 4 and 5 cyclones in the Pacific, such as Jimena, Nangka, Dolphin, Noul, Chan_Hom, and Ignacio. We find the maximum wind speed in the retrieved SMAP data within about 80 km from the eye. The location of the eye is interpolated from the BT analysis to the time of SMAP observations.

The time series comparison of SMAP's maximum wind speed with the BT analysis is illustrated in Figure 11 (left panel) for Jimena. We find that the variation of SMAP maximum wind speed agrees reasonably well with the temporal change of BT analyses. SMAP T_B winds indicate a maximum wind speed of 67 m/s on August 31, in excellent agreement with the BT analysis. We have also included the maximum wind speed from NCEP; as expected the NCEP wind significantly underestimates the intensity of hurricane. Similar time series comparison has been made for Joaquin, and the agreement is also reasonable although SMAP has missed the peak of Hurricane Joaquin (Fig. 11, right panel).

Figure 12 plots the SMAP maximum wind speed vs. the BT wind speed for all Category-1 or above storms. A linear regression analysis indicates a high correlation coefficient of 0.83 between the SMAP and NHC BT and a correlation of 0.80 between SMAP and JTWC. The linear regression for each is also illustrated in Fig. 12. The slope of linear regression is 0.96 for JWTC and 0.88 for NHC, suggesting that the NHC BT tends to have a slightly larger maximum

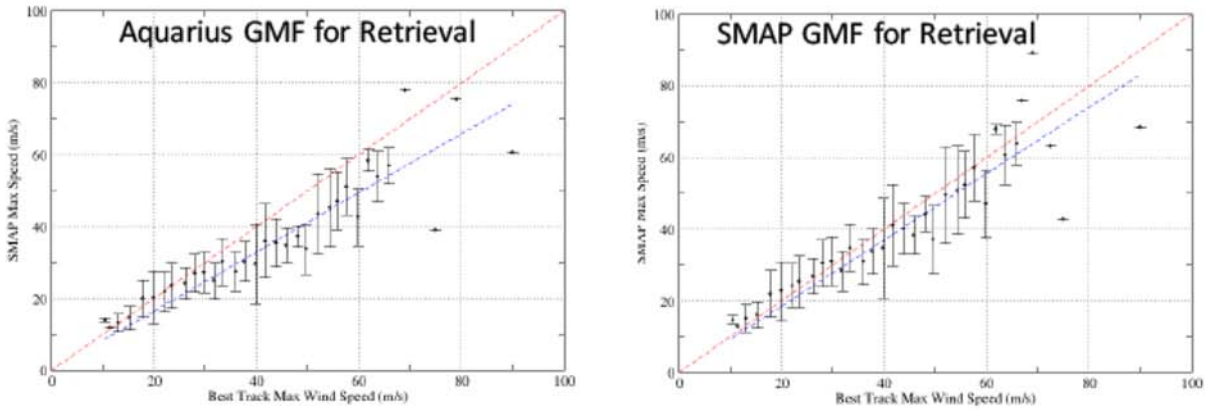

Figure 13. Comparison of the SMAP maximum wind speed derived from the SMAP and Aquarius geophysical model functions with the best track analysis from the Joint Typhoon Warning Center (JTWC) and National Hurricane Center (NHC). The red diagonal line represents the one to one reference. The black dots with uncertainty bars (one standard deviation) are the binned data. Blue dashed lines correspond to the linear regression of the binned SMAP-Best Track data. The slope of the linear regression is 0.82 based on the Aquarius model, and 0.92 based on the SMAP GMF. The SMAP radiometer shows ability for wind retrieval up to about 70 m/s.

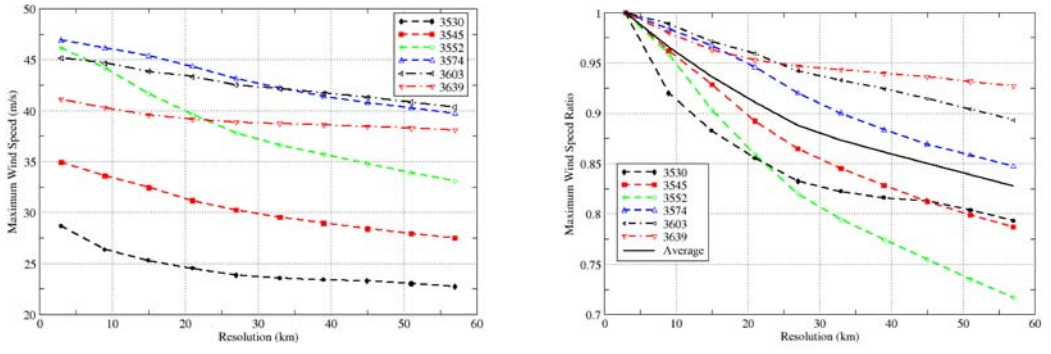

Figure 14. Spatial averaging effects on maximum wind speed are estimated from the APSU winds for Joaquin (Table 1). Left panel on the maximum wind speed vs. spatial resolution. Right panel on the maximum wind speed at a reduced resolution normalized by the maximum wind speed at 3 km spatial resolution.

wind speed than JTWC. If we take all the data without separating the NHC and JTWC BT analyses, the correlation is 0.81 and the linear regression curve is

$$W_{SMAP} = 0.93 W_{BT} \quad (4)$$

Here W_{SMAP} is the maximum wind speed from SMAP, and W_{BT} represents the 1-minute sustained maximum wind speed from the best track from JTWC or NHC.

We have performed an uncertainty analysis by grouping the SMAP maximum wind speeds in BT wind speed bins at 2 m/s intervals. For each wind speed bin, we compute the mean of the grouped SMAP maximum wind speeds ($\overline{W}_{SMAP}$) and the mean of BT wind speed ($\overline{W}_{BT}$). We have also computed the standard deviation of the grouped data in each bin. The mean and standard deviation are illustrated in Fig. 13 for retrievals using the SMAP and Aquarius GMFs. The average of standard deviations for the maximum wind speed bins greater than 20 m/s is 7.4 m/s for retrieval using the SMAP GMF. This is a very similar value compared to what was found from SMOS data at similar spatial resolution [2]. The regression of the mean with the BT wind is

$$\overline{W}_{SMAP} = 0.92 \overline{W}_{BT} \quad (5)$$

The slope of regression is very close to the regression using the data without binning (Eq. 4). This suggests that the estimated slope is sufficiently robust, not affected by non-uniform distribution of data points in the conditional wind speed bins.

The binned SMAP maximum wind speed retrieved using the Aquarius GMF is also included in Fig. 13. The corresponding linear regression is

$$\overline{W}_{SMAP-AQGMF} = 0.82 \overline{W}_{BT} \quad (6)$$

The slope of regression is about 10 percent lower than that derived using the SMAP GMF for retrieval, consistent with

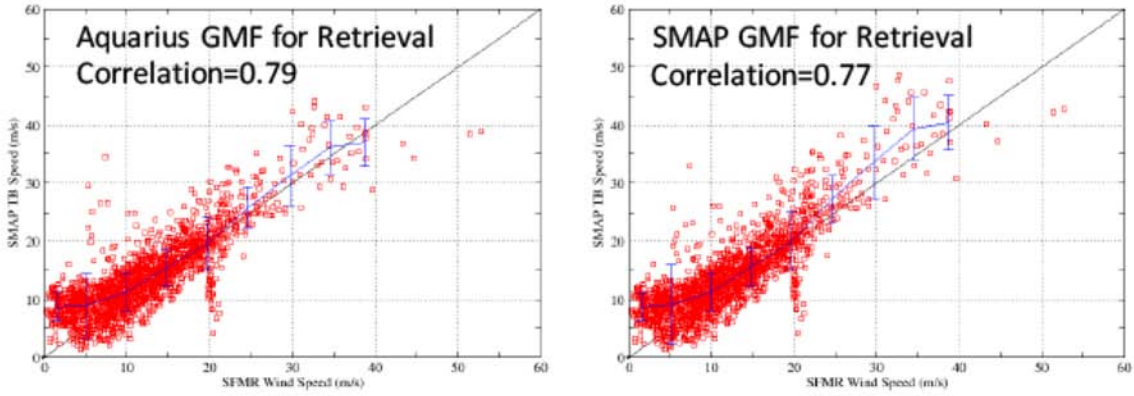

Figure 15. Comparison of SMAP and SFMR wind speeds. Left panel for the SMAP wind retrieved using the Aquarius GMF; right panel for the retrieval using the SMAP GMF. The SFMR wind speed has been averaged over the SMAP WVC resolution. Red squares represent individual SMAP-SFMR matchups. Blue lines with vertical bars indicate the conditional mean and one standard deviation.

the difference between the Aquarius and SMAP GMFs illustrated in Figs. 1 and 4.

The difference from the BT analysis in maximum wind speed could be due to the effect of spatial averaging. SMAP T_B wind represents a spatial average of winds over about 60 km. A spatial average will reduce the maximum wind on the eye wall. Furthermore, the SMAP resolution frequently cannot resolve the eye of hurricanes. See Fig. 8 for examples. An average over the wind speed on the eye wall and neighboring regions with lower wind speeds will reduce the estimation of maximum wind speed.

We examine the effects of spatial averaging by applying a moving window at various resolutions (integral numbers of 3 km) to the APSU-Joaquin 3-km winds for smoothing. The maximum wind speed in the reduced resolution image is illustrated versus the window size in Fig. 14 for six APSU winds (Table 1). Degrading the spatial resolution from 3 km to 51 km can reduce the maximum wind speed by a very wide range from 3 to 20 m/s. The worst reduction appears in the APSU analysis for SMAP rev3552D; the corresponding wind image in Fig. 3 reveals a thin eyewall with a width of about 30 km – a factor of two smaller than the wind processing resolution. In contrast, the reduction in maximum wind speed is only about 3 m/s in the APSU wind for SMAP rev 3639D, which has a high wind region extending over about 80 to 100 km (Fig. 3) – larger than the wind processing resolution. The reduction in maximum wind speed clearly depends on the relative spatial scale of eyewall and wind processing resolution. We normalize the maximum wind speed for each reduced resolution by the maximum wind speed at 3 km resolution. The ratios are illustrated in the right panel of Fig. 14. We find that the mean of ratios for six APSU winds at a spatial resolution of 57 km is about 0.83, which is strikingly close to the regression slope indicated in Eq. (6) for the winds retrieved using the Aquarius GMF.

A similar conclusion has been drawn from the smoothing of H*Wind analysis, which has a gridded resolution of about 6 km. After the smoothing of 300 H*Wind analyses to a resolution of 43 km for SMOS wind processing [2], we find that the maximum wind speed reduces by an average of about 15 percent. The reduction shown in Fig. 14 based on a limited number of APSU winds is in excellent agreement with the spatial averaging of H*Wind.

One more note is that the regression analysis shown in Fig. 13 does not support the parabolic rise of the SMOS excess T_B at the wind speeds of higher than 40 m/s (Fig. 5). Should the rising feature in the SMOS GMF be used to process the SMAP data, the maximum wind speed will reduce by about 20-30 percent or more. This will bring the SMAP maximum wind speed significantly away from the best track estimate. A larger discrepancy from best track does not necessarily mean that SMOS is less accurate because of the intrinsic differences between the spatially averaged winds from SMAP and the 1-min sustained maximum wind from best track. As discussed earlier, the discrepancy in SMOS and SMAP GMFs could be caused by differences in the reference wind data and differing range of incidence angles. It is crucial to recognize that the maximum wind speed from best track analysis cannot be used as the metric for accuracy assessment because of its fundamental differences from SMOS and SMAP satellite winds, in particular the spatial averaging effects. Future comparative analyses of SMAP and SMOS GMFs should include more extensive matchup with the same wind reference data and limit the range of SMOS data to near the incidence angle of 40 degrees.

An alternate method for validation of the SMAP wind speed is to make comparison with the wind speed products from the operational airborne SFMR [21]. We collocated the SMAP wind data with the SFMR winds, which were acquired during the 2015 hurricane season and obtained from the

National Hurricane Center. Because the time of SFMR observations could be frequently different from the time of SMAP passes by a few hours, we adjusted the location of each SFMR observation for matchup with the location of SMAP WVC based on the motion of hurricanes estimated from the best track and the time difference. We found that there were only two SFMR data above 30 m/s and within 15 min of the SMAP passes, and therefore it is important to recognize that the change of hurricane winds between the SMAP and SFMR passes will contribute to the difference between SMAP and SFMR winds. Fig. 15 illustrates the scatter of the SMAP-SFMR collocations for results obtained using Aquarius GMF for retrieval (left panel) or SMAP GMF (right panel). The correlation coefficients are very good, 0.79 for Aquarius GMF and 0.77 for SMAP GMF. We also conditionally binned the SMAP wind speed data on the SFMR winds at 5 m/s intervals. For wind speeds between 20 to 40 m/s, the mean bias is ~1.3 m/s and the mean of standard deviations is ~4.4 m/s for the Aquarius-GMF-based retrieval. The results derived from the SMAP GMF have a similar value for the mean standard deviation, but a larger positive bias. The comparison with the SFMR winds corroborate the best track analysis and supports the feasibility of retrieving hurricane wind speeds from SMAP data for at least up to 40 m/s.

V. SUMMARY

We have analyzed the SMAP radiometer data for ocean surfaces and find that the data agree reasonably well with the radiometer model functions of wind effects on excess brightness temperatures derived from the Aquarius data for low to about 20 ms^{-1} wind speeds. The collocated analysis of SMAP data and the APSU winds for Hurricane Joaquin further supports the linear extrapolation of SMAP and Aquarius GMF to hurricane force winds and the SMOS GMF [1,2]. The discrepancy with the SMOS GMF at wind speeds greater than 40 m/s requires further investigation but is very likely related to the choice of the reference wind used for building up the GMF (spatially smoothed H*WIND at ~50 km resolution in [2] versus APSU wind in the present work).

We have implemented the wind retrieval algorithms using two look radiometer data from SMAP for wind speed and direction retrieval with an effective spatial resolution of 60 km. The RMSD of wind speed with WindSat/SSMIS is 1.7 m/s, and the RMSD of wind direction is 18 degrees with respect to ECMWF for wind speeds in the range of 12 to 30 m/s. The comparison with the SFMR winds indicates an RMSD of about 4.6 m/s (root square sum of bias and standard deviation) for wind speeds in the range of 20 to 40 m/s.

The time series comparison with the best track analysis indicates that the SMAP radiometer data have a good skill to track the temporal evolution of hurricane and storm force winds. The correlation of the maximum wind speed with the best track analysis is very good, about 0.80 with JTWC and 0.83 with NHC. The slope of regression is about 0.92 using the SMAP GMF for retrieval or about 0.82 using the Aquarius GMF for retrieval, meaning that the maximum wind speed estimated from SMAP is about 8 to 18 percent lower than the best track, which appears to be consistent with the reduction due to spatial averaging effect. Our results support the findings obtained from the SMOS data that the passive L-band radiometer data can provide good estimation of hurricane wind speeds [1,2].

It is important to note that the wind direction retrieved from SMAP radiometer data above 30 m/s remains un-validated due to a lack of accurate wind direction for error assessment. One possible data source for validation is the wind direction from dropsondes, which are frequently deployed during NHC aircraft flights. This is a subject for future research.

REFERENCES

[1] Reul, N., Tenerelli, J., Chapron, B., Vandemark, D., Quilfen, Y., and Kerr, Y , "SMOS satellite L-band radiometer: A new capability for ocean surface remote sensing in hurricanes, " J. Geophysical Research-Oceans, Volume: 117, DOI: 10.1029/2011JC007474, FEB 2 2012.

[2] N. Reul, B. Chapron, E. Zabolotskikh, C. Donlon, Y. Quilfen, S. Guimbard, J.F. Piolle, A revised L-band radio-brightness sensitivity to extreme winds under tropical cyclones: The 5 year SMOS-Storm database, Remote Sensing of Environemnt, 180, 274-291. http://doi.org/10.1016/j.rse.2016.03.011

[3] D. Entekhabi, E. G. Njoku, P. E. O'Neill, K. H. Kellogg, W. T. Crow, W. N. Edelstein, J. K. Entin, S. D. Goodman, T. J. Jackson, J. Johnson, J. Kimball, J. R. Piepmeier, R. D. Koster, N. Martin, K. C. McDonald, M. Moghaddam, S. Moran, R. Reichle, J. C. Shi, M. W. Spencer, S. W. Thurman, L. Tsang, and J. Van Zyl, The Soil Moisture Active Passive (SMAP) Mission, Proceedings of IEEE, Vol. 98,No. 5,pp. 704-716, May 2010.

[4] Font, J., A. Camps, A. Borges, M. Martin-Neira, J. Boutin, N. Reul, Y. H. Kerr, A. Hahne, and S. Mecklenburg. SMOS: The Challenging Sea Surface Salinity Measurement from Space, Proceedings of the IEEE, Vol. 98, No. 5, doi: 10.1109/jproc.2009.2033.

[5] NCEP Global Forecast System products, http://nomads.ncdc.noaa.gov/data.php#hires_weather_datasets

[6] WindSat and SSMI/S products produced by the Remote Sensing System, http://www.ssmi.com/

[7] Chassignet, E.P., H.E. Hurlburt, E.J. Metzger, O.M. Smedstad, J. Cummings, G.R. Halliwell, R. Bleck, R. Baraille, A.J. Wallcraft, C. Lozano, H.L. Tolman, A. Srinivasan, S. Hankin, P. Cornillon, R. Weisberg, A. Barth, R. He, F. Werner, and J. Wilkin, 2009. U.S. GODAE: Global Ocean Prediction with the HYbrid Coordinate Ocean Model (HYCOM). Oceanography, 22(2), 64-75.

[8] Reynolds, R. W., T. M. Smith, C. Liu, D. B. Chelton, K. S. Casey, and M. G. Schlax, "Daily high-resolution blended analyses for sea surface temperature," *J. Climate*, **20**, 5473-5496, 2007.

[9] Yueh, S. H., W. Tang, A. Fore, A. Hayashi, Y. T. Song, and G. Lagerloef, "Aquarius geophysical model function and combined active passive algorithm for ocean surface salinity and wind retrieval", *J. Geophys. Res. Oceans*, 119, 5360–5379, doi:10.1002/2014JC009939, 2014.

[10] Yueh, S. H., W. Tang, A. Fore, G. Neumann, A. Hayashi, A. Freedman, J. Chaubell, and G. Lagerloef, 2013, L-band Passive and Active Microwave Geophysical Model Functions of Ocean Surface Winds and Applications to Aquarius Retrieval. *IEEE Trans. Geoscience and Remtoe Sensing*, 51 (9), 4619-4632, DOI: 10.1109/TGRS.2013.2266915.

[11] Zhang, F., and Y. Weng, 2015: Predicting Hurricane Intensity and Associated Hazards: A Five-Year Real-Time Forecast Experiment with Assimilation of Airborne Doppler Radar Observations. Bulletin of the American Meteorological Society, 96, 25-32.

[12] Weng, Y. and F. Zhang, 2016: Advances in Convection-permitting Tropical Cyclone Analysis and Prediction through EnKF Assimilation of Reconnaissance Aircraft Observations. Journal of Metrological Society of Japan, 94, doi:10.2151/jmsj. 2016-018.

[13] Simon H. Yueh, Steve Dinardo, Alexander Fore, and Fuk Li, "Passive and Active L-Band Microwave Observations and Modeling of Ocean

Surface Winds", IEEE Trans. Geosci. And Remote Sensing, Vol. 48, No. 8, pp. 3087-3100, August 2010.

[14] Powell, M. D., Houston, S. H., Amat, L. R., & Morisseau-Leroy, N. (1998). The HRD real-time hurricane wind analysis system. Journal of Wind Engineering and Industrial Aerodynamics, 77–78, 53–64. http://dx.doi.org/10.1016/S0167-6105(98)00131-7.

[15] A. G. Fore, B. W. Stiles, A. H. Chau, B. A. Williams, R. S. Dunbar and E. Rodríguez, "Point-Wise Wind Retrieval and Ambiguity Removal Improvements for the QuikSCAT Climatological Data Set," in *IEEE Transactions on Geoscience and Remote Sensing*, vol. 52, no. 1, pp. 51-59, Jan. 2014. doi: 10.1109/TGRS.2012.2235843.

[16] Piepmeier, J. R., P. Mohammed, G. De Amici, E. Kim, J. Peng, and C. Ruf, SMAP Algorithm Theoretical Basis Document: L1B Radiometer Product: Includes L1A and L1B. SMAP Project, NASA GSFC SMAP-006, NASA Goddard Space Flight Center, Greenbelt, MD. (http://nsidc.org/data/docs/daac/smap/sp_l1b_tb/pdfs/SMAP_ATBD_RadiometerL1B_TB_REV-B_20150401.pdf), 2016.

[17] Yueh, S. H., "Estimates Of Faraday Rotation With Passive Microwave Polarimetry For Microwave Remote Sensing Of Earth Surfaces," IEEE Trans. Geosci. Remote Sensing, Vol. 38, No. 5, 2434-2438, September 2000.

[18] Yueh, S. H., W. Wilson, S. Dinardo, and S. V. Hsiao, Polarimetric microwave wind radiometer model function and retrieval testing for WindSat, IEEE Trans. Geosci. Remote Sens., 44(2), 584–596, 2006.

[19] Scott J. Shaffer, R. Scott Dunbar, S. Vincent Hsiao, and David G. Long, A Median-Filter-Based Ambiguity Removal Algorithm For NSCAT, IEEE Trans. Geosci. Remote Sens., Vol. 29. No. 1. Pp. 167-174, January 1991.

[20] B. Stiles, B. Pollard, and R. Dunbar, "Direction interval retrieval with thresholded nudging: a method for improving the accuracy of QuikSCAT winds," IEEE Transactions on Geoscience and Remote Sensing, vol. 40, no. 1, pp. 79–89, January 2002.

[21] Uhlhorn, E. W., P. G. Black, J. L. Franklin, M.Goodberlet, J. Carswell and A. S. Goldstein, "Hurricane surface wind measurements from an operational stepped frequency microwave radiometer," Mon. Wea. Rev., 135 (9):3070-3085, 2007.